Original Article

A multiparameter diagnostic model based on 2-[^{18}F]FDG PET/CT metabolic parameters and clinical variables can differentiate high-risk and non-high-risk pediatric neuroblastoma under the revised Children's Oncology Group classification system

Yanfeng Xu[1#], Yukun Si[2#], Jun Liu[1], Siqi Li[1], Wei Wang[1], Guanyun Wang[1], Jigang Yang[1]

[1]Nuclear Medicine Department, Beijing Friendship Hospital, Capital Medical University, Beijing, China; [2]UItrasonic Diagnosis Department, Beijing Friendship Hospital, Capital Medical University, Beijing, China

Contributions: (I) Conception and design: G Wang, J Yang, W Wang; (II) Administrative support: Y Xu, Y Si, G Wang, J Yang; (III) Provision of study materials or patients: Y Xu Y Si, J Liu, S Li, G Wang; (IV) Collection and assembly of data: Y Xu, Y Si, W Wang, S Li; (V) Data analysis and interpretation: Y Xu, Y Si, J Liu; (VI) Manuscript writing: All authors; (VII) Final approval of manuscript: All authors.

[#]These authors contributed equally to this work.

Correspondence to: Guanyun Wang, MD; Jigang Yang, MD. PhD. Nuclear Medicine Department, Beijing Friendship Hospital, Capital Medical University, 95 Yong'an Road, Xicheng District, Beijing 100050, China. Email: 852791126@qq.com; yangjigang@ccmu.edu.cn.

Background: It is crucial to assist neuroblastoma (NB) pediatric patients in accurate risk stratification based on the revised Children's Oncology Group (COG) classification system through non-invasive examinations. This study assessed the diagnostic efficacy of integrating multiparametric 2-[^{18}F]fluoro-D-glucose positron emission tomography/computed tomography (2-[18F]FDG PET/CT) metabolic parameters with clinical variables to differentiate between high- and non-high-risk pediatric NB according to the revised COG classification system.

Methods: A retrospective study was conducted involving a total of 89 pediatric NB patients, including 71 high-risk and 18 non-high-risk patients, who underwent pre-treatment 2-[^{18}F]FDG PET/CT imaging. All patients were confirmed by pathology, and clinical variables were collected. The metabolic parameters of 2-[^{18}F]FDG PET/CT were evaluated, including maximum standard uptake value (SUVmax), mean standard uptake value (SUVmean), metabolic tumor volume (MTV) and total lesion glycolysis (TLG). The differences in diagnostic efficacy were evaluated by comparing the differences between receiver operating characteristic (ROC) curves. The DeLong test, integrated discrimination improvement (IDI), and net reclassification improvement (NRI) were utilized to assess the enhancement in diagnostic performance. The clinical utility of the diagnostic model was evaluated through decision curve analysis (DCA).

Results: The ROC curve analysis of TLG showed the highest differentiating diagnostic value [sensitivity =0.620, 95% confidence interval (CI): 0.496–0.730; specificity =0.833, 95% CI: 0.577–0.956; area under the curve (AUC) 0.764, 95% CI: 0.648–0.881; cut-off =234.70] among metabolic parameters of 2-[^{18}F]FDG PET/CT. After multivariate forward stepwise logistic regression (LR) analysis, the combined diagnostics model of age, gender, the International Neuroblastoma Risk Group Staging System (INRGSS) stage (L1/L2 *vs.* M/MS) and TLG resulted in the highest AUC of 0.932 (95% CI: 0.867–0.998; sensitivity =0.901, 95% CI: 0.802–0.956; specificity =0.889, 95% CI: 0.604–0.978). Compared to TLG, the diagnostic efficiency of the model demonstrated a significant improvement [Z=3.089, P<0.001; IDI =0.388, P<0.001; NRI (categorical) =0.736, P<0.001]. The DCA further validated the clinical efficacy of the model.

Conclusions: The multiparameter diagnosis model based on 2-[^{18}F]FDG PET/CT metabolic parameters and clinical parameters had excellent value in the differential diagnosis of high- and non-high-risk pediatric

NB under the revised COG classification system.

Keywords: Positron emission tomography (PET); neuroblastoma (NB); high-risk; metabolic parameters; the revised Children's Oncology Group classification system

Submitted Jun 03, 2024. Accepted for publication Dec 31, 2024. Published online Feb 18, 2025.
doi: 10.21037/qims-24-1111
View this article at: https://dx.doi.org/10.21037/qims-24-1111

Introduction

Neuroblastoma (NB) arises from the neural crest cells of the adrenal medulla and is the most prevalent and lethal extracranial solid malignancy in pediatric patients (1,2). The clinical behavior of NB exhibits a wide range of heterogeneity, encompassing spontaneous regression as well as resistance to treatment, metastasis, and mortality (3). Therefore, accurate prediction of patient outcomes and stratification of patient risk are crucial for tailoring treatment plans specifically designed for NB patients. The Children's Oncology Group (COG) Risk Classifier (version 1) based on the International Neuroblastoma Staging System (INSS) was established in 2000 (4), but its application has been limited due to it being postoperative staging method (5). The International Neuroblastoma Risk Group Staging System (INRGSS) relies on imaging-defined risk factors (IDRF) determined before treatment, upon which the INRG risk stratification system was constructed (6). However, the INRG classifier was developed using patient data from decades ago, so it did not consider the impact of more advanced treatments on outcomes (7). In recent years, studies have found that segmental chromosomal aberrations (SCAs) which involve the loss or acquisition of chromosome arms indicate unfavorable outcomes (8-11). The revised COG risk classifier (version 2) has been proposed for clinical guidance of NB, mainly based on INRG and SCAs in 2021 (7). However, due to the high heterogeneity of NB, there may be biases in the pathological and genetic detection indicators used for defining the risk group of NB patients obtained through invasive biopsy (12). Therefore, it is crucial to perform accurate risk stratification for patients with NB in through non-invasive examinations.

2-[^{18}F]fluoro-D-glucose positron emission tomography ^{18}F-fluorodeoxyglucose positron emission tomography/computed tomography (2-[^{18}F]FDG PET/CT) is increasingly used in pediatric malignancies (13), including NB, for diagnosis staging and predicting prognosis (14-17). The clinical application of metabolic parameters of 2-[^{18}F]FDG PET, including maximum standardized uptake value (SUVmax), mean standardized uptake value (SUVmean), total lesion glycolysis (TLG), and metabolic tumor volume (MTV), in NB has been confirmed (15,18,19). Therefore, first, our study analyzed the clinical value of metabolic parameters of 2-[^{18}F]FDG PET/CT for noninvasively identifying high- and non-high-risk pediatric NB under the revised COG classification system; Second, we developed a differential diagnosis model to distinguish between high- and non-high-risk pediatric NB under the revised COG classification system. This model integrates clinical variables with metabolic parameters derived from 2-[^{18}F]FDG PET/CT imaging. Further, we evaluated the performance of model. We present this article in accordance with the TRIPOD reporting checklist (available at https://qims.amegroups.com/article/view/10.21037/qims-24-1111/rc).

Methods

Patients

This retrospective cohort study was approved by the Institutional Review Board of Beijing Friendship Hospital (approval number: 2020-P2-091-02) and informed consent was provided by the guardians of all patients for this retrospective study. This study was performed in accordance with the Declaration of Helsinki (as revised in 2013). Guardians of all patients provided informed consent before 2-[^{18}F]FDG PET/CT was conducted.

In this study, we conducted a retrospective analysis of the imaging data from all pediatric patients diagnosed with NB who underwent 2-[^{18}F]FDG PET/CT scans prior to treatment at Beijing Friendship Hospital between March 2018 and November 2019. The inclusion criteria were as follows: (I) all patients were diagnosed by pathology; (II) no anti-tumor treatment before 2-[^{18}F]FDG PET/CT examination; (III) complete clinical data records to assign risk groups according to the revised COG classification system (7). The exclusion criteria

were as follows: (I) no pathological diagnosis obtained; (II) anti-tumor treatment before 2-[^{18}F]FDG PET/CT examination; (III) incomplete clinical data. According to INRGSS (6), patients were divided into L1, L2, M, and MS stages; patients were classified into favorable histology (FH) and unfavorable histology (UFH) according to the International Neuroblastoma Pathology Classification (INPC) (20). According to the revised COG classification system (7), we divided the NB patients into high- and non-high-risk groups. The clinical variables, including age (months), gender, primary lesion site (adrenal or extra-adrenal), *MYCN* status (amplified or not amplified), deletion of the short arm of chromosome 1p36 (normal or abnormal), deletion of the short arm of chromosome 11q (normal or abnormal), and histopathological typing (ganglioneuroblastoma, differentiated NB and poorly differentiated NB) were collected.

Image acquisition

Patients were required to undergo a fasting period of at least 6 hours. During this time, their blood glucose levels were verified to be below 11.1 mmol/L prior to the administration of 2-[^{18}F]FDG at a dose of 3.5–4.5 MBq/kg. At 60–90 minutes post-injection, all patients underwent 2-[^{18}F]FDG PET/CT imaging using a Biograph mCT scanner (Siemens Healthineers, Erlangen, Germany). Whole-body PET scans were performed to encompass the region extending from the base of the skull to the proximal femur while patients were in a free-breathing state. The parameters for PET include a 3-dimensional (3D) mode, a bed interval of 2–2.5 minutes (with 30% overlap), a bed count of 4–5 per person, 3 iterations, 21 subsets, and a Gaussian filter half-height width of 4.0 millimeters. The voltage range is 120–140 kV, the current is 100 mAs, the rotation time is 0.8 seconds, the layer thickness is 3–5 mm, and the pitch value is 1. The automatic dose modulation of the above parameters is applied to collect low-dose CT images of the whole body for attenuation correction. Image reconstruction is performed utilizing an ordered subset expectation maximization (OSEM) algorithm, incorporating CT-based attenuation correction (AC).

Image analysis

2-[^{18}F]FDG PET/CT images were evaluated using 3D Slicer software (version 4.13.0; https://www.slicer.org/) by two experienced nuclear medicine physicians (Y.X. and Y.S.) who were unaware of the patients' clinical data. NBs exhibiting abnormal 2-[^{18}F]FDG uptake on PET imaging were identified as primary lesions. The software automatically generated contours encompassing the target lesion within its boundaries, and we manually delineated 2-dimensional (2D) regions of interest (ROIs) in conjunction with these contours to form 3D volumes of interest (VOIs). For quantitative MTV measurement, we selected regions within lesions where the standardized uptake value (SUV) intensity exceeded 40% of the SUVmax. Metabolic PET variables included the primary lesion SUVmax and primary lesion SUVmean.

Statistical analysis

The categorical variables were reported as frequencies and percentages [n (%)] in order to provide a qualitative description of the data. For continuous variables with normal distribution, independent sample *t*-test [mean± standard deviation (SD)] was used for comparison; Mann-Whitney *U* test [median (interquartile range)] was used to represent skewed continuous variables. The Kolmogorov-Smirnov test was utilized to evaluate the normality of the distribution of data. To evaluate the predicted values of PET parameters, we quantified the area under the receiver operating characteristic (ROC) curve (AUC) to identify the optimal PET parameters for differential diagnosis. Additionally, we calculated sensitivity, specificity, positive predictive value (PPV), and negative predictive value (NPV). Multivariate logistic regression (LR) analysis was utilized to construct diagnostic models for distinguishing between the high- and the non-high-risk group. Multivariate LR analysis was employed to develop diagnostic models for discriminating between the non-high- and high-risk group. The DeLong test, integrated discriminatory improvement (IDI), and net reclassification improvement (NRI) were employed to compare the diagnostic performance of the model with the PET parameters that demonstrated the highest AUC. This comparison aimed to evaluate the differential diagnostic performance between the PET parameters and the diagnostic model. The clinical utility and accuracy of the model were assessed using decision curve analysis (DCA), which evaluates the net benefit across a range of threshold probabilities, focusing on the interval with the highest AUC (21). The DeLong test was conducted using the *pROC* package, and IDI and NRI were performed with the *PredictABEL* package. The DCA was performed with the *rmda* package. Commercial software

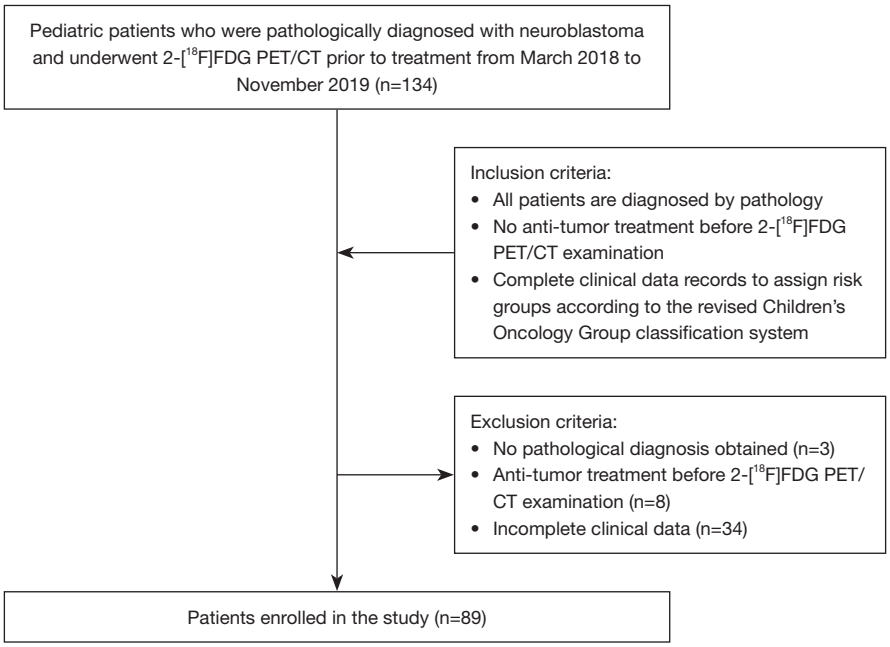

Figure 1 Patient inclusion and exclusion flow diagram. After the inclusion and exclusion criteria had been applied, a total of 89 pediatric patients with neuroblastoma were included in our study. 2-[^{18}F]FDG PET/CT, 2-[^{18}F]fluoro-D-glucose positron emission tomography/computed tomography.

including SPSS 24.0 (IBM Corp., Armonk, NY, USA) and R software program version 4.0.2 (R Foundation for Statistical Computing, Vienna, Austria) were used to perform statistical analysis on the data. All statistical tests were two-tailed with a significance level set at P=0.05.

Results

Clinical variables

A total of 89 pediatric patients with NB were included in our study, including 71 high-risk patients and 18 non-high-risk patients (*Figure 1*). The clinical variables between high-risk patients and non-high-risk patients are presented in *Table 1*.

Regarding clinical variables, a significant difference was observed in age (45.9±27.4 *vs.* 30.2±18.4 months, P=0.024) and gender [boy/girl: 36 (51%)/35 (49%) *vs.* 4 (22%)/14 (78%), P=0.039] between high-risk patients and non-high-risk patients. The INRGSS stage [L1: 0 (0%) *vs.* 12 (67%); L2: 11 (15.5%) *vs.* 3 (17%); M: 58 (82%) *vs.* 3 (17%); MS: 2 (3%) *vs.* 0 (0%), P<0.001], MYCN amplification [34 (48%) *vs.* 3 (17%), P=0.007], deletion of the short arm of chromosome 11q [abnormal: 36 (51%) *vs.* 2 (11%), P=0.002] and INPC [FH/UFH: 13 (18%)/58 (82%) *vs.* 13 (72%)/5 (28%), P<0.001] between high-risk patients and non-high-risk patients. However, there was no statistical difference in primary lesion site [adrenal: 52 (73%) *vs.* 10 (56%), P=0.145], deletion of the short arm of chromosome 1p36 [abnormal: 38 (53.5%) *vs.* 14 (78%), P=0.062], and pathological histological typing [ganglioneuroblastoma: 30 (42%) *vs.* 7 (39%); differentiated NB: 9 (13%) *vs.* 4 (22%); poorly differentiated NB: 32 (45%) *vs.* 7 (39%), P=0.589] between high- and non-high-risk patients.

Comparison of 2-[^{18}F]FDG PET/CT metabolic parameters between high- and non-high-risk patients

Compared with high-risk patients, the metabolic parameters of 2-[^{18}F]FDG PET/CT in patients with non-high-risk patients, including SUVmax (5.38±2.76 *vs.* 3.73±2.41, P=0.023), MTV [165.48 (78.07–357.21) *vs.* 59.19 (6.67–107.56), P=0.001] and TLG [381.77 (146.31–805.68) *vs.* 126.65 (6.44–213.24), P=0.001] were significantly higher. However, there was no statistical difference in SUVmean between the two groups (SUVmean: 2.31±1.03 *vs.* 1.86±1.15, P=0.114). The 2-[^{18}F]FDG PET/CT metabolic

Table 1 Patient clinical variables between high-risk neuroblastoma patients and non-high-risk neuroblastoma patients

Variables	High-risk (n=71)	Non-high-risk (n=18)	P value
Age (months)	45.9±27.4	30.2±18.4	0.024
Boy/girl	36 [51]/35 [49]	4 [22]/14 [78]	0.039
Primary lesion site			0.145
Adrenal	52 [73]	10 [56]	
Extra-adrenal	19 [27]	8 [44]	
INRGSS stage			<0.001
L1	0 [0]	12 [67]	
L2	11 [15.5]	3 [17]	
M	58 [82]	3 [17]	
MS	2 [3]	0 [0]	
MYCN status			0.007
Amplified	34 [48]	3 [17]	
Not amplified	37 [52]	15 [83]	
1p36			0.062
Normal	38 [53.5]	14 [78]	
Abnormal	33 [46.5]	4 [22]	
11q			0.002
Normal	35 [49]	16 [89]	
Abnormal	36 [51]	2 [11]	
International Neuroblastoma Pathology Classification			<0.001
FH	13 [18]	13 [72]	
UFH	58 [82]	5 [28]	
Histopathological typing			0.589
Ganglioneuroblastoma	30 [42]	7 [39]	
Differentiated neuroblastoma	9 [13]	4 [22]	
Poorly differentiated neuroblastoma	32 [45]	7 [39]	

Data are presented as mean ± standard deviation or n [%]. INRGSS, International Neuroblastoma Risk Group Staging System; FH, favorable histology; UFH, unfavorable histology.

parameters between high-risk patients and non-high-risk patients are summarized in *Table 2*.

The differential diagnostic performance of 2-[^{18}F]FDG PET metabolic parameters and model in high- and non-high-risk patients

Table 3 presents the diagnostic performance of 2-[^{18}F]FDG PET metabolic parameters and models in high- versus non-high-risk patients. The ROC curve analysis revealed that TLG exhibited the highest diagnostic accuracy among the 2-[^{18}F]FDG PET metabolic parameters, with a cut-off value of 234.70 g and an AUC of 0.764 [95% confidence interval (CI): 0.648–0.881]. The results showed that the sensitivity was 0.620 (95% CI: 0.496–0.730), the specificity was 0.833 (95% CI: 0.577–0.956), the PPV was 0.936 (95% CI: 0.814–0.983), and the NPV was 0.357 (95% CI: 0.220–0.520). Meanwhile, according to the difference in 2-[^{18}F]

Table 2 The difference of 2-[^{18}F]FDG PET/CT metabolic parameters between high-risk neuroblastoma patients and non-high-risk neuroblastoma patients

Variables	High-risk (n=71)	Non-high-risk (n=18)	P value
SUVmax	5.38±2.76	3.73±2.41	0.023
SUVmean	2.31±1.03	1.86±1.15	0.114
MTV (mL)	165.48 (78.07–357.21)	59.19 (6.67–107.56)	0.001
TLG (g)	381.77 (146.31–805.68)	126.65 (6.44–213.24)	0.001

Data are presented as mean ± standard deviation or median (interquartile range). 2-[^{18}F]FDG PET/CT, 2-[^{18}F]fluoro-D-glucose positron emission tomography/computed tomography; SUVmax, max standard uptake value; SUVmean, mean standard uptake value; MTV, metabolic tumor volume; TLG, total lesion glycolysis.

Table 3 Differential diagnostic efficiency of 2-[^{18}F]FDG PET/CT metabolic parameters and different diagnostic models between high-risk neuroblastoma patients and non-high-risk neuroblastoma patients

Parameters	Cut-off	AUC	Sensitivity	Specificity	PPV	NPV
SUVmax	3.28	0.707 (0.559–0.856)	0.845 (0.735–0.916)	0.556 (0.313–0.776)	0.882 (0.776–0.944)	0.476 (0.264–0.697)
SUVmean	1.53	0.672 (0.521–0.824)	0.845 (0.735–0.916)	0.500 (0.268–0.732)	0.870 (0.762–0.935)	0.450 (0.238–0.680)
MTV (mL)	88.94	0.758 (0.635–0.881)	0.704 (0.582–0.804)	0.778 (0.519–0.926)	0.926 (0.813–0.976)	0.400 (0.244–0.578)
TLG (g)	234.70	0.764 (0.648–0.881)	0.620 (0.496–0.730)	0.833 (0.577–0.956)	0.936 (0.814–0.983)	0.357 (0.220–0.520)
Model	–	0.932 (0.867–0.998)	0.901 (0.802–0.956)	0.889 (0.604–0.978)	0.970 (0.885–0.995)	0.667 (0.431–0.845)

Data are presented as (95% CI). Model: age (>30 months) plus gender (boy) plus INRGSS stage (M/MS) plus TLG (>234.7). 2-[^{18}F]FDG PET/CT, 2-[^{18}F]fluoro-D-glucose positron emission tomography/computed tomography; SUVmax, max standard uptake value; SUVmean, mean standard uptake value; MTV, metabolic tumor volume; TLG, total lesion glycolysis; AUC, area under the curve; PPV, positive predictive value; NPV, negative predictive value; CI, confidence interval; INRGSS, International Neuroblastoma Risk Group Staging System.

Table 4 Comparison of the TLG and model to with Delong test, IDI and NRI

Variable	Delong test		IDI (95% CI)	P value	NRI (95% CI)	P value
	Z	P value				
Model *vs*. TLG	3.089	0.002	0.388 (0.271–0.506)	<0.001	0.736 (0.530–0.941)	<0.001

Model: age (>30 months) plus gender (boy) plus INRGSS stage (M/MS) plus TLG (>234.7). TLG, total lesion glycolysis; IDI, integrated discrimination improvement; NRI, net reclassification improvement (categorical); CI, confidence interval.

FDG PET/CT metabolic parameters between high- and non-high-risk patients, based on multivariate LR analysis, we constructed a diagnostic model. In the diagnostic model, the clinical variables included age (>30 *vs.* ≤30 months), gender (boy *vs.* girl), INRGSS stage (M/MS *vs.* L1/L2), and TLG (>234.7). The model showed that the AUC was 0.932 (95% CI: 0.867–0.998), the sensitivity was 0.901 (95% CI: 0.802–0.956), the specificity was 0.889 (95% CI: 0.604–0.978), and the PPV and NPV were 0.970 (95% CI: 0.885–0.995), and 0.667 (95% CI: 0.431–0.845), respectively. The model is shown below.

$$y = \frac{1}{1+e^{-(1.29\times[\text{age}>30\text{ months}]+1.24\times[\text{boy}]+3.35\times[\text{INRGSS stage M/MS}]+2.64\times[\text{TLG}>234.7]-2.42)}} \quad [1]$$

The model allowed for a significant reclassification, with an IDI of 0.388 (95% CI: 0.271–0.506, P<0.001) and a categorical NRI of 0.736 (0.530–0.941, P<0.001), compared to TLG alone. The Delong test indicated that the AUC of the model was significantly higher than that of TLG (Z=3.089, P=0.002). These findings, as presented in *Table 4*, highlight the advantages of employing a multiparametric approach in statistical diagnostics for distinguishing

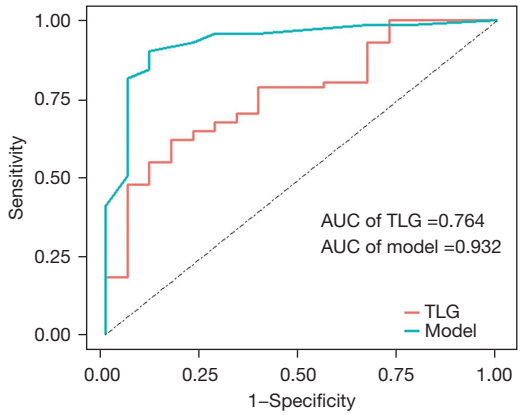

Figure 2 The predictive value of 2-[^{18}F]fluoro-D-glucose positron emission tomography/computed tomography parameters and diagnostic model [including age (>30 months) plus gender (boy) plus International Neuroblastoma Risk Group Staging System stage (M/MS) plus TLG (>234.7)] was assessed by quantifying the AUCs. The areas under the ROC curves for the ability to differentiate high-risk patients and non-high-risk patients for TLG was 0.764 (95% CI: 0.648–0.881, cut-off: 234.70 g, sensitivity: 0.620, specificity: 0.833, PPV: 0.936, and NPV: 0.357) and for model was 0.932 (95% CI: 0.867–0.998, sensitivity: 0.901, specificity: 0.889, PPV: 0.970, and NPV: 0.667), respectively. AUC, area under the curve; TLG, total lesion glycolysis; ROC, receiver operating characteristic; CI, confidence interval; PPV, positive predictive value; NPV, negative predictive value.

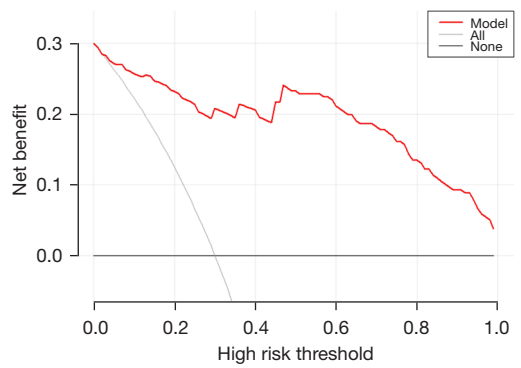

Figure 3 DCA for combined diagnostic model [including age (>30 months) plus gender (boy) plus International Neuroblastoma Risk Group Staging System stage (M/MS) plus TLG, >234.7]. The DCA indicates that, irrespective of the threshold probability considered by either clinicians or patients, employing the combined diagnostic model from this study for differentiating between high- and non-high-risk patients is valuable. DCA, decision curve analysis; TLG, total lesion glycolysis.

between high- and non-high-risk patients. The diagnostic efficiencies of TLG and model are shown in *Figure 2* and *Table 3*. According to the Delong test, compared with TLG, the model had a statistically significant improvement in ROC (Z=3.889, P<0.001).

Clinical application

The DCA for the model is illustrated in *Figure 3*. The DCA indicated that the model achieved a significant net benefit across the entire range of risk thresholds.

Discussion

Our study results suggested that 2-[^{18}F]FDG PET/CT metabolic parameters could distinguish high- and non-high-risk pediatric patients with NB based on the revised COG classification system. Combining clinical variables age (>30 months), gender (boy), INRGSS stage (M/MS), with 2-[^{18}F]FDG PET/CT metabolic parameters (TLG >234.7) could better distinguish high-risk and non-high-risk pediatric patients with NB based on the revised COG classification system.

The high heterogeneity of NB hinders the successful development of high-risk NB treatment, with non-high-risk NB patients having a 5-year survival rate of over 90%, whereas high-risk NB patients have a 5-year survival rate between 20% and 50% (22,23). The management of high-risk NB necessitates the formulation of a comprehensive therapeutic regimen encompassing chemotherapy, radiotherapy, and surgery (24). On the original COG classification system, the revised COG classification system was proposed, incorporating prognostic factors for NB, including *MYCN* status, ploidy, INPC histology, and SCAs at 1p36 and 11q (7). However, the risk stratification of NB typically necessitates the utilization of invasive pathological and genetic testing (25). Additionally, pathology and bone marrow biopsy are employed to determine the underlying histopathological subtype of NB as well as the presence of bone marrow involvement; however, reliance on fine-needle biopsy, which is commonly used, largely depends on the number of samples obtained and manual operations may introduce sampling errors (26). Therefore, it is crucial to develop non-invasive methods for risk stratification in NB patients to guide treatment and predict prognosis accurately.

The application of nuclear medicine in NB has been confirmed, especially for disease staging and treatment evaluation (13). As the most commonly

used nuclear medicine examination technique, I-123 metaiodobenzylguanidine (^{123}I-mIBG) scans has high sensitivity and specificity (27). However, 10% of NB are non-mIBG avid, and the spatial resolution of ^{123}I-mIBG imaging is relatively low, which limits the diagnosis of smaller lesions. 2-[^{18}F]FDG PET/CT can partially address the aforementioned issues, and current studies have demonstrated that 2-[^{18}F]FDG PET/CT holds clinical value in the diagnosis, staging, predicting pathological classification, and *MYCN* copy number category, monitoring response during treatment, and prognosis prediction of NB (5,28-30). A phase I study compared 139 lesions identified on concomitant 2-[^{18}F]FDG PET/CT and MIBG scans. The overall concordance of positive lesions between the two scans was 39.6%. Notably, although MIBG scan exhibited significantly higher sensitivity in detecting individual lesions in relapsed NB, 2-[^{18}F]FDG PET/CT occasionally played a complementary role, particularly for soft tissue lesions (31). It should be noted that complete response determined by metabolic evaluation using 2-[^{18}F]FDG PET/CT did not always correlate with complete response based on MIBG uptake. A recent study retrospectively analyzed a cohort of 39 consecutive pediatric patients with newly diagnosed stage 4 NB who underwent both baseline and post-chemotherapy 2-[^{18}F]FDG PET/CT imaging. It was observed that patients achieving complete resolution on PET (no residual 2-[^{18}F]FDG uptake higher than the surrounding backgrounds) after chemotherapy exhibited significantly improved 5-year OS compared to those without complete resolution (73.6% *vs.* 39.0%, P=0.044) (32). These findings provide evidence supporting the utility of 2-[^{18}F]FDG PET/CT in assessing treatment response among children with stage 4 NB. However, experience with 2-[^{18}F]FDG PET/CT in NB is still limited.

Importantly, NB is a highly heterogeneous tumor, and 2-[^{18}F]FDG PET/CT, as a multimodal imaging technique, has broad prospects for non-invasive exploration of tumor heterogeneity (33). Our study demonstrated the clinical significance of 2-[^{18}F]FDG PET/CT metabolic parameters in discriminating between high- and non-high-risk NB patients, with TLG exhibiting superior diagnostic efficacy (AUC =0.764, 95% CI: 0.648–0.881). The TLG is considered a more comprehensive parameter compared to SUV parameters, as it better reflects the metabolic tumor burden (34). Previous studies have demonstrated that TLG could predict the prognosis and status of NB patients with the *MYCN* oncogene and chromosome 1p36, all of which are related to the revised COG classification system (19,35). The *MYCN* oncogene and chromosome 1p36 in the revised COG classification system were also correlated with prognosis. Meanwhile, research has also found that compared to advanced (III–IV) NB lesions, early-stage (I–II) NB may have lower FDG metabolism (36). These findings may explain why TLG could effectively distinguish between high- and non-high-risk NB patients. However, considering the heterogeneity of NB and the non-specific uptake of FDG by primary lesions, relying solely on metabolic parameters to distinguish high- and non-high-risk NB may not be accurate enough.

To date, there has only been one study on the application of imaging methods to distinguish high- and non-high-risk patients based on the revised COG classification system. Wang *et al.* conducted a relevant study using a radiomics signature based on CT (25). Their findings demonstrated that the construction of radiomics models utilizing linear discriminant analysis (LDA), LR, and support vector machine (SVM) achieved an AUC exceeding 0.8 in both the training and validation datasets. Compared to the above study, when we combined clinical variables with 2-[^{18}F]FDG PET/CT metabolic parameters to construct a diagnostic model, including age (>30 months), gender (boy), INRGSS stage (M/MS), and TLG (>234.7), higher diagnostic efficacy could be achieved (AUC =0.932). The model constructed by our study achieved excellent sensitivity (0.950) and specificity (1.000), enabling more accurate and non-invasive identification of high-risk NB patients. Considering that the revised COG classification system often requires invasive testing and a combination of multiple tests to distinguish between high- and non-high-risk pediatric with NB, we only used clinical data (age and gender) and imaging examinations (INRGSS stage and TLG) from NB patients to non-invasively and simply distinguish the degree of risk, and demonstrated high diagnostic ability. This can provide assistance for patients' clinical decision-making and might influence patient management (*Figure 4*).

There are still many limitations in this study: (I) the study was limited by a small sample size and its retrospective design, conducted solely at a single center; (II) our study only analyzed the primary lesion and did not consider any metastatic lesions; (III) the measurement of 2-[^{18}F]FDG PET/CT metabolic parameters may be influenced by multiple factors, which may lead to the non-repeatability of diagnostic models; (IV) our study only analyzed 2-[^{18}F]FDG PET/CT metabolic parameters, and other parameters such as textural parameters and radiomics signatures were not included in our study. The validation of our study

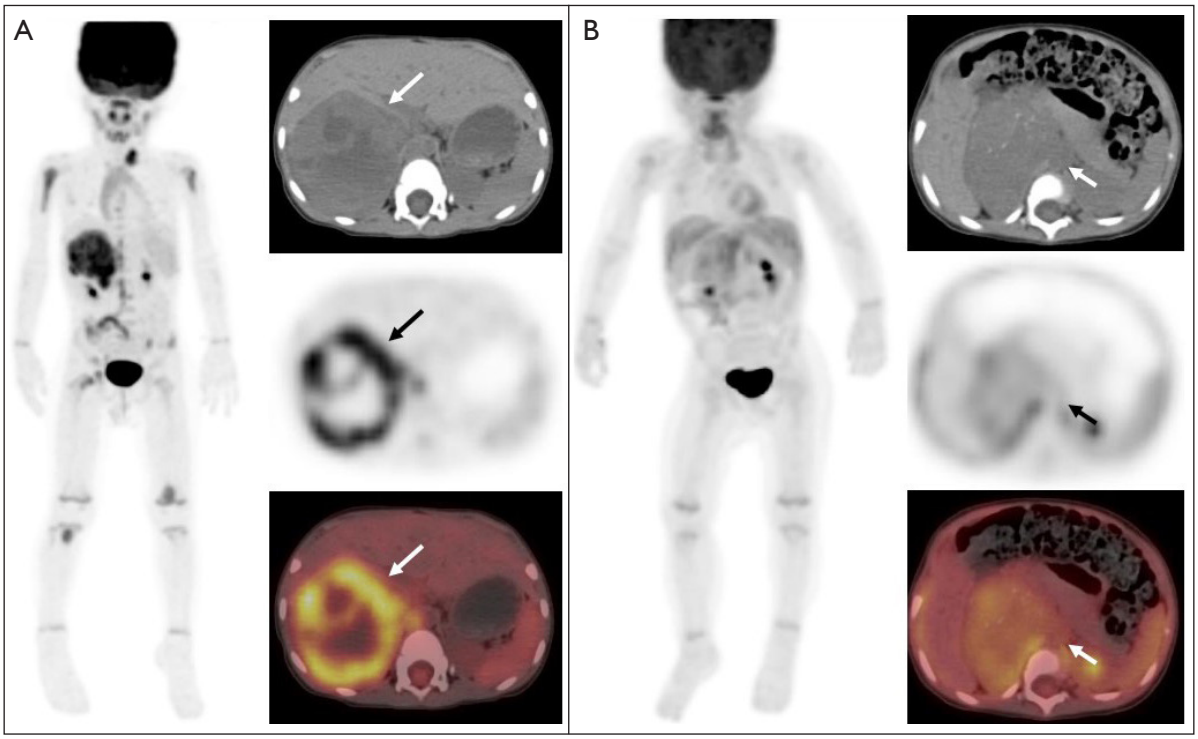

Figure 4 2-[^{18}F]FDG PET/CT of pediatric patients diagnosed with high- and low-risk neuroblastoma by the combined diagnostic model. (A) A 2-year-old boy was diagnosed with high-risk neuroblastoma characterized by *MYCN* amplification and multiple bone metastases [the arrows in (A) indicate the main lesion]. Despite undergoing surgery chemotherapy and immunotherapy, the disease still progressed and ultimately resulting in death. (B) A 1-year-old girl was diagnosed with low-risk neuroblastoma by the combined diagnostic model [the arrows in (B) indicate the main lesion]. The girl achieved complete remission following surgical intervention and chemotherapy, with no evidence of recurrence during the 30-month follow-up period. 2-[^{18}F]FDG PET/CT, 2-[^{18}F]fluoro-D-glucose positron emission tomography/computed tomography.

findings necessitates the implementation of larger sample sizes and multicenter studies in subsequent investigations to enhance the diagnostic capability, stability, and repeatability of the model. At the same time, we can incorporate textural parameters and radiomic signals into future study, which can help to more accurately distinguish between high- and non-high-risk pediatrics with NB.

Conclusions

Our findings demonstrated that 2-[^{18}F]FDG PET/CT metabolic parameters could non-invasively distinguish high- and non-high-risk pediatric patients diagnosed with NB based on the revised COG classification system. The model, combining clinical variables [age (>30 months), gender (boy), INRGSS stage (M/MS)], and with 2-[^{18}F]FDG PET/CT metabolic parameters [TLG (>234.7)] could better non-invasively distinguish high- and non-high-risk pediatric patients with NB based on the revised COG classification system. Our findings can assist in the non-invasive identification of high-risk NB patients, providing more guidance for NB patients treatment management and prognosis.

Acknowledgments

The authors would like to thank the staff at Nuclear Medicine Department, Beijing Friendship Hospital, Affiliated to Capital Medical University for their assistance in carrying out this study.

Footnote

Reporting Checklist: The authors have completed the

TRIPOD reporting checklist. Available at https://qims.amegroups.com/article/view/10.21037/qims-24-1111/rc

Funding: This study was supported by grants from National Natural Science Foundation of China (Nos. 82272034, 82001860, 81971642, and 82001861).

Conflicts of Interest: All authors have completed the ICMJE uniform disclosure form (available at https://qims.amegroups.com/article/view/10.21037/qims-24-1111/coif). The authors have no conflicts of interest to declare.

Ethical Statement: The authors are accountable for all aspects of the work in ensuring that questions related to the accuracy or integrity of any part of the work are appropriately investigated and resolved. This retrospective cohort study was approved by the the Institutional Review Board of Beijing Friendship Hospital (approval No. 2020-P2-091-02). Informed consent was provided by the guardians of all patients for this retrospective study. This study was conducted in accordance with the Declaration of Helsinki (as revised in 2013).

References

1. Smith MA, Seibel NL, Altekruse SF, Ries LA, Melbert DL, O'Leary M, Smith FO, Reaman GH. Outcomes for children and adolescents with cancer: challenges for the twenty-first century. J Clin Oncol 2010;28:2625-34.
2. Trigg RM, Shaw JA, Turner SD. Opportunities and challenges of circulating biomarkers in neuroblastoma. Open Biol 2019;9:190056.
3. Chung C, Boterberg T, Lucas J, Panoff J, Valteau-Couanet D, Hero B, Bagatell R, Hill-Kayser CE. Neuroblastoma. Pediatr Blood Cancer 2021;68 Suppl 2:e28473.
4. Liang WH, Federico SM, London WB, Naranjo A, Irwin MS, Volchenboum SL, Cohn SL. Tailoring Therapy for Children With Neuroblastoma on the Basis of Risk Group Classification: Past, Present, and Future. JCO Clin Cancer Inform 2020;4:895-905.
5. Lanza C, Galeazzi V, Carboni N, De Berardinis A, De Marino L, Barile A, Giovagnoni A. Neuroblastoma image-defined risk factors in adrenal neuroblastoma: role of radiologist. Gland Surg 2019;8:S168-77.
6. Monclair T, Brodeur GM, Ambros PF, Brisse HJ, Cecchetto G, Holmes K, Kaneko M, London WB, Matthay KK, Nuchtern JG, von Schweinitz D, Simon T, Cohn SL, Pearson AD; . The International Neuroblastoma Risk Group (INRG) staging system: an INRG Task Force report. J Clin Oncol 2009;27:298-303.
7. Irwin MS, Naranjo A, Zhang FF, Cohn SL, London WB, Gastier-Foster JM, Ramirez NC, Pfau R, Reshmi S, Wagner E, Nuchtern J, Asgharzadeh S, Shimada H, Maris JM, Bagatell R, Park JR, Hogarty MD. Revised Neuroblastoma Risk Classification System: A Report From the Children's Oncology Group. J Clin Oncol 2021;39:3229-41.
8. Janoueix-Lerosey I, Schleiermacher G, Michels E, Mosseri V, Ribeiro A, Lequin D, Vermeulen J, Couturier J, Peuchmaur M, Valent A, Plantaz D, Rubie H, Valteau-Couanet D, Thomas C, Combaret V, Rousseau R, Eggert A, Michon J, Speleman F, Delattre O. Overall genomic pattern is a predictor of outcome in neuroblastoma. J Clin Oncol 2009;27:1026-33.
9. Attiyeh EF, London WB, Mossé YP, Wang Q, Winter C, Khazi D, McGrady PW, Seeger RC, Look AT, Shimada H, Brodeur GM, Cohn SL, Matthay KK, Maris JM; . Chromosome 1p and 11q deletions and outcome in neuroblastoma. N Engl J Med 2005;353:2243-53.
10. Schleiermacher G, Michon J, Ribeiro A, Pierron G, Mosseri V, Rubie H, et al. Segmental chromosomal alterations lead to a higher risk of relapse in infants with MYCN-non-amplified localised unresectable/disseminated neuroblastoma (a SIOPEN collaborative study). Br J Cancer 2011;105:1940-8.
11. Schleiermacher G, Mosseri V, London WB, Maris JM, Brodeur GM, Attiyeh E, Haber M, Khan J, Nakagawara A, Speleman F, Noguera R, Tonini GP, Fischer M, Ambros I, Monclair T, Matthay KK, Ambros P, Cohn SL, Pearson AD. Segmental chromosomal alterations have prognostic impact in neuroblastoma: a report from the INRG project. Br J Cancer 2012;107:1418-22.
12. Schmelz K, Toedling J, Huska M, Cwikla MC, Kruetzfeldt LM, Proba J, et al. Spatial and temporal intratumour heterogeneity has potential consequences for single biopsy-based neuroblastoma treatment decisions. Nat

Commun 2021;12:6804.
13. Samim A, Tytgat GAM, Bleeker G, Wenker STM, Chatalic KLS, Poot AJ, Tolboom N, van Noesel MM, Lam MGEH, de Keizer B. Nuclear Medicine Imaging in Neuroblastoma: Current Status and New Developments. J Pers Med 2021;11:270.
14. Liu J, Si Y, Zhou Z, Yang X, Li C, Qian L, Feng LJ, Zhang M, Zhang SX, Liu J, Kan Y, Gong J, Yang J. The prognostic value of (18)F-FDG PET/CT intra-tumoural metabolic heterogeneity in pretreatment neuroblastoma patients. Cancer Imaging 2022;22:32.
15. Man S, Yan J, Li J, Cao Y, Hu J, Ma W, Liu J, Zhao Q. Value of pretreatment 18F-FDG PET/CT in prognosis and the reflection of tumor burden: a study in pediatric patients with newly diagnosed neuroblastoma. Int J Med Sci 2021;18:1857-65.
16. Feng L, Zhang S, Lu X, Yang X, Kan Y, Wang C, Zhang H, Wang W, Yang J. An Optimal Radiomics Nomogram Based on (18)F-FDG PET/CT for Identifying Event-Free Survival in Pediatric Neuroblastoma. Acad Radiol 2023;30:2309-20.
17. Feng L, Zhang S, Wang C, Li S, Kan Y, Wang C, Zhang H, Wang W, Yang J. Axial Skeleton Radiomics of (18)F-FDG PET/CT: Impact on Event-Free Survival Prediction in High-Risk Pediatric Neuroblastoma. Acad Radiol 2023;30:2487-96.
18. Li C, Zhang J, Chen S, Huang S, Wu S, Zhang L, Zhang F, Wang H. Prognostic value of metabolic indices and bone marrow uptake pattern on preoperative 18F-FDG PET/CT in pediatric patients with neuroblastoma. Eur J Nucl Med Mol Imaging 2018;45:306-15.
19. Hu R, Zhang Y, Liu S, Lee P, Liu C, Liu A. Prognostic prediction by (18)F-FDG-PET/CT parameters in patients with neuroblastoma: a systematic review and meta-analysis. Front Oncol 2023;13:1208531.
20. Shimada H, Ambros IM, Dehner LP, Hata J, Joshi VV, Roald B, Stram DO, Gerbing RB, Lukens JN, Matthay KK, Castleberry RP. The International Neuroblastoma Pathology Classification (the Shimada system). Cancer 1999;86:364-72.
21. Zhang Z, Rousson V, Lee WC, Ferdynus C, Chen M, Qian X, Guo Y; written on behalf of AME Big-Data Clinical Trial Collaborative Group. Decision curve analysis: a technical note. Ann Transl Med 2018;6:308.
22. Matthay KK, Maris JM, Schleiermacher G, Nakagawara A, Mackall CL, Diller L, Weiss WA. Neuroblastoma. Nat Rev Dis Primers 2016;2:16078.
23. Whittle SB, Smith V, Doherty E, Zhao S, McCarty S, Zage PE. Overview and recent advances in the treatment of neuroblastoma. Expert Rev Anticancer Ther 2017;17:369-86.
24. Swift CC, Eklund MJ, Kraveka JM, Alazraki AL. Updates in Diagnosis, Management, and Treatment of Neuroblastoma. Radiographics 2018;38:566-80.
25. Wang H, Xie M, Chen X, Zhu J, Ding H, Zhang L, Pan Z, He L. Development and validation of a CT-based radiomics signature for identifying high-risk neuroblastomas under the revised Children's Oncology Group classification system. Pediatr Blood Cancer 2023;70:e30280.
26. Schriegel F, Taschner-Mandl S, Bernkopf M, Grunwald U, Siebert N, Ambros PF, Ambros I, Lode HN, Henze G, Ehlert K. Comparison of three different methods to detect bone marrow involvement in patients with neuroblastoma. J Cancer Res Clin Oncol 2022;148:2581-8.
27. Matthay KK, Shulkin B, Ladenstein R, Michon J, Giammarile F, Lewington V, Pearson AD, Cohn SL. Criteria for evaluation of disease extent by (123) I-metaiodobenzylguanidine scans in neuroblastoma: a report for the International Neuroblastoma Risk Group (INRG) Task Force. Br J Cancer 2010;102:1319-26.
28. Brink A, Hlongwa KN, More S. The Impact of PET/CT on Paediatric Oncology. Diagnostics (Basel) 2023;13:192.
29. Qian LD, Feng LJ, Zhang SX, Liu J, Ren JL, Liu L, Zhang H, Yang J. (18)F-FDG PET/CT imaging of pediatric peripheral neuroblastic tumor: a combined model to predict the International Neuroblastoma Pathology Classification. Quant Imaging Med Surg 2023;13:94-107.
30. Qian LD, Zhou ZA, Li SQ, Liu J, Zhang SX, Ren JL, Wang W, Yang J. (18)F-fluorodeoxyglucose ((18)F-FDG) positron emission tomography/computed tomography (PET/CT) imaging of pediatric neuroblastoma: a multi-omics parameters method to predict MYCN copy number category. Quant Imaging Med Surg 2024;14:3131-45.
31. Taggart DR, Han MM, Quach A, Groshen S, Ye W, Villablanca JG, Jackson HA, Mari Aparici C, Carlson D, Maris J, Hawkins R, Matthay KK. Comparison of iodine-123 metaiodobenzylguanidine (MIBG) scan and [18F]fluorodeoxyglucose positron emission tomography to evaluate response after iodine-131 MIBG therapy for relapsed neuroblastoma. J Clin Oncol 2009;27:5343-9.
32. Lu X, Li C, Wang S, Yin Y, Fu H, Wang H, Cheng W, Chen S. The prognostic role of (18)F-FDG PET/CT-based response evaluation in children with stage 4 neuroblastoma. Eur Radiol 2024;34:7125-35.

33. Chicklore S, Goh V, Siddique M, Roy A, Marsden PK, Cook GJ. Quantifying tumour heterogeneity in 18F-FDG PET/CT imaging by texture analysis. Eur J Nucl Med Mol Imaging 2013;40:133-40.
34. Gill R, Abdah-Bortnyak R, Amit A, Bar-Peled U, Keidar Z. [F18]FDG PET/CT-Derived Metabolic and Volumetric Biomarkers Can Predict Response to Treatment in Locally Advanced Cervical Cancer Patients. Cancers (Basel) 2022;14:4382.
35. Ren J, Fu Z, Zhao Y. Clinical value of (18)F-FDG PET/CT to predict MYCN gene, chromosome 1p36 and 11q status in pediatric neuroblastoma and ganglioneuroblastoma. Front Oncol 2023;13:1099290.
36. Choi YJ, Hwang HS, Kim HJ, Jeong YH, Cho A, Lee JH, Yun M, Lee JD, Kang WJ. (18)F-FDG PET as a single imaging modality in pediatric neuroblastoma: comparison with abdomen CT and bone scintigraphy. Ann Nucl Med 2014;28:304-13.

Cite this article as: Xu Y, Si Y, Liu J, Li S, Wang W, Wang G, Yang J. A multiparameter diagnostic model based on 2-[^{18}F] FDG PET/CT metabolic parameters and clinical variables can differentiate high-risk and non-high-risk pediatric neuroblastoma under the revised Children's Oncology Group classification system. Quant Imaging Med Surg 2025;15(3):2094-2105. doi: 10.21037/qims-24-1111